

nnMobileNet: RETHINKING CNN FOR RETINOPATHY RESEARCH

Wenhui Zhu^{1*}, Peijie Qiu^{2*}, Xin Li¹, Natasha Lepore³, Oana M. Dumitrascu⁴, Yalin Wang¹

¹ School of Computing and Augmented Intelligence, Arizona State University, AZ 85281, USA

² McKeley School of Engineering, Washington University in St. Louis, St. Louis, MO 63130, USA

³ CIBORG Lab, Department of Radiology Children’s Hospital Los Angeles, Los Angeles, CA 90027, USA

⁴ Department of Neurology, Mayo Clinic, Scottsdale, AZ 85251, USA

ABSTRACT

Over the past few decades, convolutional neural networks (CNNs) have been at the forefront of the detection and tracking of various retinal diseases (RD). Despite their success, the emergence of vision transformers (ViT) in the 2020s has shifted the trajectory of RD model development. The leading-edge performance of ViT-based models in RD can be largely credited to their scalability—their ability to improve as more parameters are added. As a result, ViT-based models tend to outshine traditional CNNs in RD applications, albeit at the cost of increased data and computational demands. ViTs also differ from CNNs in their approach to processing images, working with patches rather than local regions, which can complicate the precise identification of small, variably presented lesions in RD. In our study, we revisited and updated the architecture of a CNN model, specifically MobileNet, to enhance its utility in RD diagnostics. We found that an optimized MobileNet, through selective modifications, can surpass ViT-based models in various RD benchmarks, including diabetic retinopathy grading, detection of multiple fundus diseases, and classification of diabetic macular edema. The code is available at <https://github.com/Retinal-Research/NN-MOBILENET>

Index Terms— Retinal Diseases, Fundus image, Classification, Convolution Neural Network

1. INTRODUCTION

Retinal diseases (RD), such as diabetic retinopathy (DR), age-related macular degeneration, inherited retinal conditions, myopic maculopathy, and retinopathy of prematurity, are major contributors to blindness worldwide [2]. Deep neural networks, particularly convolutional neural networks (CNNs), have been extensively used in retinal image analysis over the past decades, achieving cutting-edge results in various RD-related tasks [3–11]. The effectiveness of CNNs in these applications is largely due to their inherent architectural inductive biases, such as spatial hierarchies, locality, and

translation invariance. These characteristics enable CNNs to transform local visual elements like edges and textures into complex, high-level abstracted features. Building on this approach, numerous CNN-based RD models [5–7, 10] have incorporated disease-specific biases into their design. However, the specialized nature of these CNN-based models for RD limits their versatility across a range of RD tasks.

Recent advancements in RD modeling [12–16] have largely revolved around the vision transformer [17] (ViT) since its debut in the 2020s. The prowess of ViT-based models in RD is primarily due to their capacity to scale effectively; their performance improves as the model size grows [18]. In addition, ViT-based models are advantageous for capturing long-range global dependencies via self-attention mechanism. Nonetheless, the quadratic time and memory complexity of self-attention operation make ViTs computationally intense and data-hungry. Accordingly, ViT-based RD models typically necessitate pretraining on large-scale datasets [12, 13, 15]. Furthermore, unlike CNNs, these models generally lack locality, since they operate at the image patch level [15].

To address these challenges, new iterations of ViT design introduce convolution-like features to recover local context sensitivity [15, 19]. This adaptation is particularly beneficial for RD research since RD tasks are typically small and have heterogeneous appearances. One representative example can be found in the DR task, where four distinct types of lesions (i.e., microaneurysms, soft exudates, hemorrhages, and hard exudates) exhibit variations in shape, size, structure, and contrast. Among these lesions, the microaneurysms are too tiny to be easily detected. In addition, the DR grading task inherently contains hierarchical information, e.g., a proliferative DR image may consist of all types of lesions. These intrinsic properties in RD tasks naturally align with inductive biases in CNNs, where hierarchical and fine-grained local contexts can be better detected than ViTs. This observation prompts a reconsideration: *could CNNs be inherently more suited to RD tasks than ViTs?*

We also note that recent studies have shown well-tuned CNNs surpassing ViTs in general image classification tasks [18].

*These authors contributed equally to this paper

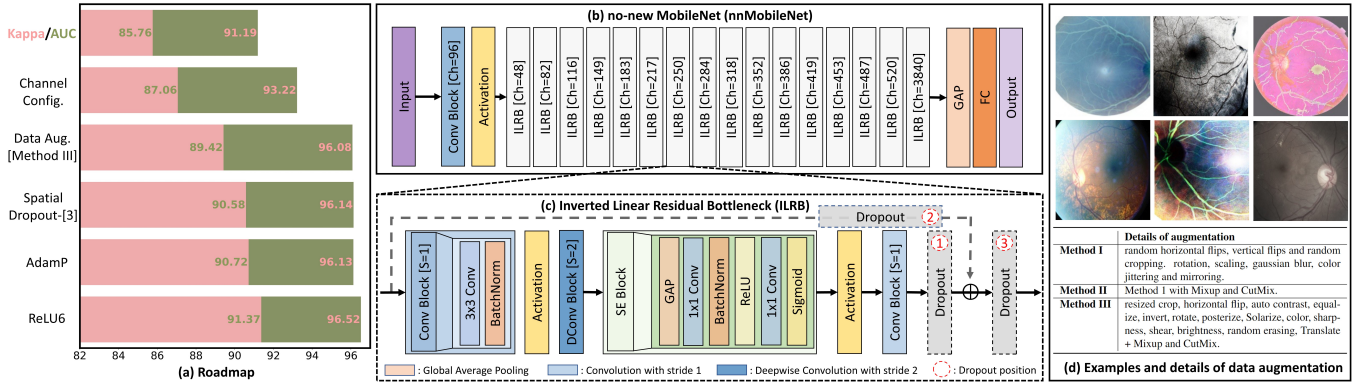


Fig. 1. (a) The roadmap of modifying a MobileNetV2 to the proposed no-new MobileNet (nnMobileNet) on the Messidor-2 dataset [1]; (b) the detailed architecture of the no-new MobileNet; (c) the inverted linear residual bottleneck used in the no-new MobileNet; and (d) examples of data augmentation (Method III) and details of three sets of data augmentation we used.

Motivated by these findings, our research recalibrated a CNN, specifically MobileNetV2, for RD applications, focusing on training methodologies and architectural refinements like the inverted bottleneck, dropout optimization, and activation functions [20]. Here, we introduce nnMobileNet (“no-new” MobileNet), a model that implements strategic, yet minimal, enhancements. Our empirical results confirmed nnMobileNet’s superiority over many leading RD models across a spectrum of benchmarks. Our work not only substantiates the potential of CNNs in RD research but also emphasizes the critical aspects of CNN optimization. We anticipate that our findings will spark a renewed interest in the adaptability and fine-tuning of CNNs within the field.

2. ROADMAP OF A NNMOBILENET

Our investigation started with a standard MobileNetV2 on the Messidor-2 dataset (Fig.1(a)) [1]. We chose MobileNetV2 because of its efficiency, achieved by replacing the traditional residual bottleneck [21] with an inverted linear residual bottleneck (ILRB) where channel attention was included by default (see Fig.1(b)). We conducted empirical studies on its key components, including channel configuration, data augmentation, dropout, optimizer, and activation functions.

2.1. Channel Configuration of ILRB

Recent findings in natural images have revealed that changing stage-wise channel configuration (primarily computation distribution between layers) led to a remarkable performance gain [18, 22]. This improvement is primarily due to two factors: first, the expressiveness of a layer is affected by the rank of its output matrix [22]. Second, ViTs generally use a different stage ratio from CNNs to change its computation distribution [18]. Both of these factors indicated the necessity of changing the channel configuration in MobileNetV2.

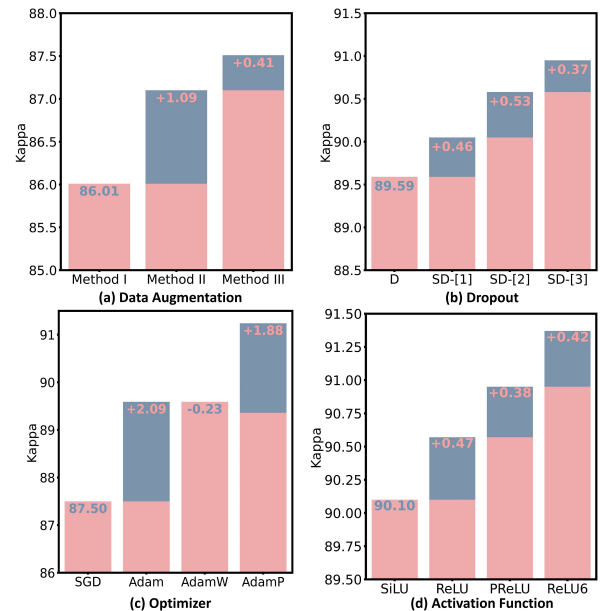


Fig. 2. Empirical studies on Messidor-2 dataset where sub-panel pictures (a), (b), (c), and (d) represent different experimental groups, each of which is independent of the others. D and SD-[x] in subpanel (b) denote Dropout and Spatial-Dropout in position [x] as shown in Fig.1(c), respectively.

As consistent with findings in natural images, we empirically found that changing the channel configuration led to a performance gain of 2.03% in Kappa and 1.30% in AUC (see the second row in Fig. 1(a)). It is worth noting that we follow the channel configuration in [22] (see Fig.1(b) for details).

2.2. Data Augmentation

In the field of RD, a common belief was that heavy data augmentation (e.g., Mixup and CutMix) should be avoided, as it dramatically distorts structures of images [5, 13, 14]. How-

ever, recent research has revealed that heavy data augmentation even boosted the performance in retinal vessel segmentation [23]. We hypothesize that this finding can be transferred to the RD tasks because the introduction of noise from the heavy data augmentation (e.g., unrealistic images shown in Fig.1(c)) may help the model generalize better. To validate those hypotheses, we conducted experiments on three different sets of data augmentation combinations from light to heavy (as detailed by Methods I, II, III in Fig.1(c)).

Interestingly, we found that the heaviest data augmentation (i.e., Method III) achieved the best performance compared to the other two strategies (see Fig. 2). We conjectured that different from ViTs which perform classification by comparing patches, the lack of non-local context in CNNs may necessitate heavy data augmentation to find the most discriminative local feature representation for abstracting heterogeneous RD lesions. Integrating this set of data augmentation into our nnMobileNet model design can improve Kappa by 2.36% and AUC by 2.86% (see the third row in Fig. 1(a)).

2.3. Dropout

Dropout is commonly employed to alleviate overfitting and enhance the representational capacity of individual layers. However, we argue that the standard Dropout [24], which randomly zeros out neurons in a feature map, is unsuitable for general RD tasks. This is mainly due to the fact that specific lesion information is primarily encoded in certain image color channels. An example can be seen in the case of DR, where the information of microaneurysm predominantly resides in the red channel, while the exudate information is primarily encoded in the green channel. Based on this observation, we conjecture that spatial Dropout, which randomly removes channels from a feature map, is a better choice for RD tasks. Additionally, spatial Dropout naturally preserves spatial and local structures by randomly dropping out strongly activated local patterns [25], which is highly needed in RD. However, *where to place spatial Dropout remains an open problem*. Here, we conducted experiments to investigate the strategic placement of spatial Dropout in ILRB (see Fig.1(c)).

We observed that i) spatial Dropout is indeed more effective than standard Dropout for RD tasks and ii) the performance varies when placing the spatial Dropout at different positions (see Fig.2(b)). Integrating spatial Dropout into the proposed model led to an improvement of 0.06% in Kappa and 1.16% in AUC (see the forth row in Fig.1(a)).

2.4. Optimizer

The training of ViTs is typically performed by an AdamW [26] optimizer, which makes us wonder if the performance gain in ViT-based RD models comes from the more advanced optimizer [18]. Alternatively, *would a more advanced optimizer boost the performance of a CNN-based RD model?*

Table 1. The detailed information of five benchmark datasets for various RD tasks we used for experiments.

Dataset	Task	Size	Metrics (%)
Messidor-1	nrDR vs rDR	1,200	AUC
Messidor-2	DR grading	1,748	{Kappa, AUC}
APOTS	DR grading	3,662	{ACC, F1, Kappa, AUC}
IDRiD	DR grading/DME	516	{ACC, F1, AUC}
RFMiD	Multi-disease Detection	3,200	{Kappa, AUC}
MMAC	Myopic Maculopathy	1,143	{SPE, F1, Kappa}

Note: The Messidor-1 dataset is mainly used for rDR classification, where Grades 0-1: non-referral DR (non-rDR) and Grades 2-3: referral DR (rDR). The MMAC dataset comes from the MICCAI myopic maculopathy analysis challenge 2023. The evaluation metrics ACC and SPE stand for accuracy and specificity, respectively.

Our empirical studies revealed that training the network with AdamP [27] optimizer, which better accommodates the step size adaptively, showed superior performance compared to other optimizers (see Figure 2). Applying the AdamP to train nnMobileNet contributed to a performance gain of 2.2% in Kappa and 0.48% in AUC (see the fifth row in Fig. 1(a)).

2.5. Activation Function

ReLU is extensively used in traditional CNNs due to its simplicity and computational efficiency. However, increasing research indicates that smoother variants of ReLU (e.g., SiLU), commonly used in ViTs, can lead to performance improvements [18, 22]. Based on that, we investigate the most suitable activation functions within inverted linear residual blocks (see Fig.1(b)) for retinal disease applications. Here, we consider four variants of ReLU, including SiLU, ReLU, PReLU, and ReLU6. As shown in Figure 2, the ReLU6 was the best among all options. After we replaced the ReLU6 in each ILRB, it led to an improvement of 0.65% in kappa and 0.39% in AUC (see the sixth row in Fig. 1(a)).

3. EXPERIMENTS AND RESULTS

All the nnMobileNet models were trained under the best settings identified in Section 2 for 1000 epochs with a L_2 weight decay of 0.05. The batch size was set to 32. The optimal initial learning rate was found to be 0.001 by random search. The learning rate was then annealed using a cosine decay scheduler after 20 linear warm-up steps. We compared the performance of the proposed nnMobileNet with state-of-the-art baselines for each RD task.

3.1. Datasets and Evaluation Metrics

To validate the proposed method, we conducted experiments on five benchmark datasets for various RD tasks including DR grading, severity classification of diabetic macular edema (DME), multi-disease abnormal detection, and myopic maculopathy grading. Details of the datasets and their corresponding RD tasks can be found in Table 1. It should be noted that we kept the same data partitions in [5, 12–14].

Table 2. Normal/non-rDR versus rDR classification on the Messidor-1 dataset. Annotations denote whether pixel-level or patch-level supervision was applied.

Method	Annotations	Referral	Normal
		AUC	AUC
Comp. CAD [9]	-	91.0	87.6
Expert A [9]	-	94.0	92.2
Expert B [9]	-	92.0	86.5
Zoom-in-Net [6]	-	95.7	92.1
AFN [8]	patch	96.8	-
Semi + Adv [7]	pixel	97.6	94.3
CANet [5]	-	96.3	-
LAT [14]	-	98.7	96.3
Ours	-	98.7	97.5

Table 3. Multi-disease detection on the RFMiD dataset.

Method	Normal/Abnormal		
	ACC	AUC	F1
CANet [5]	88.3	91.0	90.4
ReXNet [22]	91.3	94.5	93.3
CrossFormer-L [16]	90.6	94.3	92.0
Swin-L [15]	89.5	93.8	91.6
MIL-VT [12]	91.1	95.9	94.4
SatFormer-B [13]	93.8	96.5	95.8
Ours	94.4	98.7	94.4

3.2. Experimental Results

DR task performance. The proposed method achieved superior performance on the IDRID dataset compared to all baselines. Specifically, the proposed method outperformed the second-best model (DETACH+DAW [10]) by improving ACC by 23.5% and AUC by 8% (Table 5). In the APOTS dataset (see Table 4), the proposed method achieved the highest ACC (89.1) and Kappa (93.4) as well as a comparable AUC to ViT-based MIL-VT method (97.8 vs. 97.9). In addition, we achieved the same performance as the ViT-based LAT model [14] in the referral DR classification and the best performance in the normal classification (see Table 2).

Multi-disease abnormal detection performance. The proposed method achieved the best performance in terms of ACC and AUC in the RFMiD dataset (Table 3). Although the F1 score of SatFormer-B [13] was higher than ours’, the SatFormer-B [13] was a more complex ViT-based model with more parameters and computational complexity. It is worth noting that other ViT-based models (i.e., MIL-VT [12]) were pre-trained on large-scale external datasets.

DME classification performance. The proposed method achieved the best performance without any pre-training, surpassing the second-best model (DETACH+DAW [10]) in the DME classification task by 6.5% and 1.7% in AUC and Kappa, respectively (Table 5).

MICCAI MMAC 2023 Challenge. Our well-calibrated Mo-

Table 4. DR grading on the APOTS dataset.

Method	DR Grading			
	AUC	ACC	F1	Kappa
DLI [28]	-	82.5	80.3	89.0
CANet [5]	-	83.2	81.3	90.0
GREEN-ResNet50 [29]	-	84.4	83.6	90.8
GREEN-SE-ResNext50 [29]	-	85.7	85.2	91.2
MIL-VT [12]	97.9	85.5	85.3	92.0
Ours	97.8	89.1	88.9	93.4

Table 5. DR and DME grading on the IDRID dataset.

Method	DME			DR		
	AUC	F1	ACC	AUC	F1	ACC
CANet [5]	87.9	66.1	78.6	78.9	42.3	57.3
Multi-task net [30]	86.1	60.3	74.8	78	43.9	59.2
MTMR-net [31]	84.2	61.1	79.6	79.7	45.3	60.2
DETACH + DAW [10]	89.5	72.3	82.5	84.8	49.4	59.2
Ours	95.3	84.8	86.5	91.6	72.6	73.1

Table 6. MMAC official released the final ranking.

Method	Kappa	F1	SPE	Average	CPU time (s)
Rank 1 st	90.1	78.1	94.5	87.5	2.1283
Rank 2 nd	88.9	76.8	94.1	86.6	0.8047
Ours (Rank 3 rd)	90.0	75.1	94.1	86.4	0.2750

bileNet secured the third position in MICCAI MMAC 2023 Challenge [32] and was remarkably close to the top-ranking models (Table 6). Whereas models that won the first and second places were ViT-based models pre-trained on large-scale external datasets using self-supervised learning. Consequently, their models were at least three times slower than ours’ regarding the inference time on CPU (see Table 6).

4. CONCLUSION

In this paper, we proposed a series of modifications for MobileNetV2. This lightweight CNN model can outperform ViT-based and multi-task-based CNN models across multiple RD benchmarks while retaining simplicity and efficiency. It even achieved a favorable result without applying the self-supervised training technique on external datasets. The results will challenge several widely held views and prompt people to rethink the importance of convolution in RD.

5. REFERENCES

- [1] Etienne Decencière and et al., “Feedback on a publicly distributed image database: The messidor database,” *Image Analysis & Stereology*, 2014.
- [2] David Yorston, “Retinal diseases and vision 2020,” *Community Eye Health*, pp. 19–20, 2003.
- [3] Wenhui Zhu and et al. ”, “OTRE: Where optimal transport guided unpaired image-to-image translation meets

- regularization by enhancing,” in *IPMI*. Springer, 2023, pp. 415–427.
- [4] Wenhui Zhu and et al., “Optimal transport guided unsupervised learning for enhancing low-quality retinal images,” in *ISBI*, 2023, pp. 1–5.
- [5] Xiaomeng Li and et al., “CANet: Cross-Disease Attention Network for Joint Diabetic Retinopathy and Diabetic Macular Edema Grading,” *IEEE Trans Med Imaging*, pp. 1483–1493, 2020.
- [6] Zhe Wang and et al., “Zoom-in-net: Deep mining lesions for diabetic retinopathy detection,” in *MICCAI*, 2017, pp. 267–275.
- [7] Yi Zhou and et al., “Collaborative learning of semi-supervised segmentation and classification for medical images,” in *CVPR*, 2019.
- [8] Zhiwen Lin and et al., “A framework for identifying diabetic retinopathy based on anti-noise detection and attention-based fusion,” in *MICCAI*, Cham, 2018, pp. 74–82, Springer.
- [9] Clara I Sánchez and et al., “Evaluation of a computer-aided diagnosis system for diabetic retinopathy screening on public data,” *Investigative ophthalmology & visual science*, vol. 52, no. 7, pp. 4866–4871, 2011.
- [10] Haoxuan Che, Haibo Jin, and Hao Chen, “Learning robust representation for joint grading of ophthalmic diseases via adaptive curriculum and feature disentanglement,” in *MICCAI*, 2022, pp. 523–533.
- [11] Wenhui Zhu and et al., “Self-supervised equivariant regularization reconciles multiple-instance learning: Joint referable diabetic retinopathy classification and lesion segmentation,” in *18th SIPAIM*, 2023, vol. 12567, pp. 100–107.
- [12] Shuang Yu and et al., “Mil-vt: Multiple instance learning enhanced vision transformer for fundus image classification,” in *MICCAI*, 2021, pp. 45–54.
- [13] Yankai Jiang and et al., “Satformer: Saliency-guided abnormality-aware transformer for retinal disease classification in fundus image,” in *IJCAI*, 2022.
- [14] Rui Sun and et al., “Lesion-aware transformers for diabetic retinopathy grading,” in *CVPR*, 2021, pp. 10938–10947.
- [15] Yawei Li and et al., “Localvit: Bringing locality to vision transformers,” *arXiv preprint arXiv:2104.05707*.
- [16] Wenxiao Wang and et al., “Crossformer: A versatile vision transformer hinging on cross-scale attention,” *arXiv preprint arXiv:2108.00154*, 2021.
- [17] Alexey Dosovitskiy and et al., “An image is worth 16x16 words: Transformers for image recognition at scale,” *arXiv preprint arXiv:2010.11929*, 2020.
- [18] Zhuang Liu and et al., “A convnet for the 2020s,” in *Proc. IEEE Comput. Soc. Conf. Comput. Vis. Pattern Recognit*, 2022, pp. 11976–11986.
- [19] Ze Liu and et al., “Swin transformer: Hierarchical vision transformer using shifted windows,” in *ICCV*, 2021, pp. 10012–10022.
- [20] Mark Sandler and et al., “Mobilenetv2: Inverted residuals and linear bottlenecks,” in *CVPR*, 2018, pp. 4510–4520.
- [21] Kaiming He and et al., “Deep residual learning for image recognition,” in *CVPR*, 2016, pp. 770–778.
- [22] Dongyoon Han and et al., “Rethinking channel dimensions for efficient model design,” in *CVPR*, 2021, pp. 732–741.
- [23] Enes Sadi Uysal and et al., “Exploring the limits of data augmentation for retinal vessel segmentation,” *arXiv preprint arXiv:2105.09365*, 2021.
- [24] Nitish Srivastava and et al., “Dropout: a simple way to prevent neural networks from overfitting,” *The journal of machine learning research*, pp. 1929–1958, 2014.
- [25] Jonathan Tompson and et al., “Efficient object localization using convolutional networks,” in *CVPR*, 2015, pp. 648–656.
- [26] Ilya Loshchilov and Frank Hutter, “Decoupled weight decay regularization,” in *ICLR*, 2017.
- [27] Byeongho Heo and et al., “Adamp: Slowing down the slowdown for momentum optimizers on scale-invariant weights,” *ICLR*, 2020.
- [28] Alexander Rakhlin, “Diabetic retinopathy detection through integration of deep learning classification framework,” *BioRxiv*, p. 225508, 2017.
- [29] Shaoteng Liu and et al., “Green: a graph residual re-ranking network for grading diabetic retinopathy,” in *MICCAI*, 2020, pp. 585–594.
- [30] Qingyu Chen and et al., “A multi-task deep learning model for the classification of Age-related Macular Degeneration,” *AMIA Jt Summits Transl Sci Proc*, 2019.
- [31] Lihao Liu and et al., “Multi-Task Deep Model With Margin Ranking Loss for Lung Nodule Analysis,” *IEEE Trans Med Imaging*, vol. 39, no. 3, pp. 718–728, 2020.
- [32] “<https://codalab.lisn.upsaclay.fr/competitions/12441>,” .